Mem. S.A.It. Vol. 93, 188

Memorie della

Deciphering the high-energy sky via angular cross correlations
and
Unveiling Dark Matter and missing baryons in the high-energy sky

Enzo Branchini[1,12], Gabriele Parimbelli[1,2,3,4], Marco Regis[5,6], Matteo Viel[2,3,4,7], Simone Ammazzalorso[5,6], Stefano Camera[5,6,8], Manuel Colavincenzo[5,6], Xiuhui Tan[5,6,9,10,11], Marco Taoso[5].

[1] Dipartimento di Matematica e Fisica. Universitá Roma Tre and INFN, Via della Vasca Navale 84, I–00146, Roma, Italy
[2] Scuola Internazionale Superiore di Studi Avanzati, via Bonomea, 265, I–34136, Trieste, Italy
[3] INAF-OATs, Osservatorio Astronomico di Trieste, Via Tiepolo 11, I–34131 Trieste, Italy
[4] IFPU – Institute for Fundamental Physics of the Universe, Via Beirut 2, I–34151 Trieste, Italy
[5] Dipartimento di Fisica. Università di Torino, via P. Giuria 1, I–10125 Torino, Italy, e-mail: marco_regis@unito.it
The remaining affiliations can be found at the end of the paper.

Received: 9 January 2022; Accepted: 25 May 2022

Abstract.
The standard cosmological model, so successful in describing an impressively large number of observations, is characterized by the presence of unseen components that dominate the mass-energy budget of the Universe. Two of these, the Dark Matter and the "missing baryons" are key ingredients to understand the build-up of cosmic structures, their thermal and chemical history and their spatial distribution in the nearby Universe. Despite of their importance, the intrinsic properties of these components, i.e. the fundamental nature of DM and the physical status of the MB, are still unknown.
In this project, composed by two programs, we analyze the cross-correlation between distributions of objects from surveys of the large scale structure of the Universe with X-ray and γ-ray maps, in order to search for unambiguous electromagnetic signals from these two dark components.
The main outcome consists of state-of-the-art bounds on the properties of particle DM and new predictions on the spatial distribution and physical properties of the MB.

Key words. Cosmology: Observations, Dark Matter. Astrophysics: γ-ray and X-ray Astronomy

1. Introduction

Despite overwhelming gravitational evidences for dark matter [DM] at the galactic, cluster, and cosmological scales have been accumulating, still the identification of the DM nature remains one of the most challenging issues of our age in fundamental physics. At the same time, less than half of the baryonic content inferred from observations of the primordial Universe is still undetected in the Local Universe, originating the so called "missing baryon" [MB] problem.

In this project, we test the particle physics interpretation of DM by employing two signals representatives of the two sides of the particle DM coin: gravitational tracers (cosmic structures) combined with electromagnetic signals originated from DM through its self-annihilation or decay. This is achieved by computing the statistical angular cross-correlation [CC] between the two types of signal. The idea behind this approach is to use 3D maps of the gravitational potential in the Universe as a filter to be applied to γ- and X-ray maps in order to disentangle a particle DM signal from other astrophysical emissions in these energy-bands. Indeed, a stronger gravitational potential implies higher DM density and in turn brighter non-gravitational DM signal. In the standard cosmological model DM constitutes the backbone of all cosmic structures, and DM halos represent, collectively, a potential source of DM annihilation or decay signals. This means that even if the radiation from a single halo is too dim to be detected, their cumulative signal and its spatial coherence could be. In addition, since DM annihilation/decay signals peak at redshift $z < 0.3$, they can be separated by the "background" given by astrophysical processes that typically trace the star formation history and therefore peaks at higher redshifts (Regis et al. 2015).

We analyze the CC between the γ-ray *Fermi*-LAT sky and the 1-year data of cosmic shear from the Dark Energy Survey [DES] (Abbott et al. 2016; Zuntz et al. 2018; Hoyle et al. 2018; Abbott et al. 2018), reporting the first detection of a CC signal between the extragalctic γ-ray sky and the lensing signal (Ammazzalorso et al. 2020). This analysis is complemented by the study of the angular auto-correlation of the unresolved γ-ray background (UGRB) (Ackermann et al. 2018) and of the CC of the UGRB with catalogs of galaxies (Ammazzalorso et al. 2018), in order to estimate the contribution of extragalactic astrophysical sources (blazars, star-forming galaxies, active galactic nuclei) to the UGRB and to disentangle a possible DM contribution.

These results, together with those of previous studies carried out by this team (i.e. Regis et al. (2015) and Cuoco et al. (2015)), demonstrate that CC analyses can be used to detect and identify the sources of the UGRB by combining the all-sky γ-ray maps produced by the *Fermi*-LAT satellite with different tracers of the mass in the Universe.

We pushed forward this approach by considering those phenomena responsible for line emission, rather than broad band signals, and by considering other frequency bands, in particular studying the unresolved X-ray background. The latter includes a possible contribution by the so called "missing baryons", originally advocated by Fukugita et al. (1997) and later confirmed by e.g. Cen et al. (1999); Shull et al. (2012), in the warm-hot intergalactic medium (WHIM). Outside our Galaxy faint line emission in the X-ray is expected to originate from the highly ionized ions that populate the WHIM, where most of the MB are expected to reside. We recently obtained the first convincing detection of the elusive WHIM from the identification of two absorption systems in the X-ray spectrum to a quasar at $z > 0.4$ (Nicastro et al. 2018), followed by another detection of 17 absorption systems in the spectrum of another quasar at $z = 0.297$ (Kovacs et al. 2018). Going beyond the mere detection, the estimate of the MB cosmological abundance and the study of their physical properties represent one of the main science drivers of upcoming and future X-ray satellite missions capable to perform integral field spectroscopy like XRISM and Athena (XRISM Science Team 2020; Nandra et al. 2013). The detection of the oxygen lines OVII and OVIII will, in principle, allow one to perform intensity mapping analyses analogous to

those that will exploit the 21 cm line in the radio band. Emission line studies are more challenging than those based on the absorption systems because of the significant contamination from Galactic foreground and AGN (Takei et al. 2011) photons. However, like in the γ-ray case, the CC with the tracers of the large scale structures is expected to remove these contaminants since the WHIM emission is expected to be associated to the large scale structures of the Universe. In this work we use state-of-the art hydrodynamical simulations to assess how effectively a CC analysis will help studying the elusive WHIM and to estimate the possibility of performing intensity mapping using next generation X-ray datasets.

Moreover, we exploit the CC approach to seek for the line signal originated from particle DM decay. Several theories beyond the Standard Model of particle physics predict the existence of DM particles with mass in the keV range, most notably sterile neutrinos. They can provide a component of warm DM and their radiative decay would contribute to the X-ray background. With the intensity mapping technique and CC analysis with galaxy surveys we are able to test, in particular, the DM interpretation of a possibly unidentified line at 3.55 keV, as well as the case of sterile neutrino as DM in a broader range of masses (Caputo et al. 2020).

Finally, we use cross correlation analysis to study two further possible dark components: a population of primordial black holes [PBHs] and axion-like particles. The first one is constrained from the deviation it can cause on the matter power spectrum (Murgia et al. 2019). This topic is particularly important given the increasing number of VIRGO-LIGO events and the possibility that PBHs could represent a fraction or the whole DM. Axion-like DM is one of the mostly studied particle solution to the DM problem and we investigated whether an eV-axion can explain the "puzzling" auto-correlation angular power spectrum of the near infrared sky (Caputo et al. 2021).

2. The UGRB and WIMPs

Using the DES Y1 weak lensing catalogue and the *Fermi*-LAT 9-year γ-ray data, we report the first detection of the cross-correlation between the γ-ray sky and the gravitational lensing shear, with a significance of SNR= 5.3. The bulk of this signal comes from the correlation of point-like γ-ray sources with their host halo. The energy spectrum of the signal is hard, and most likely dominated by blazars. In addition, we find a hint for a cross-correlation on large scales. Its spectral and redshift behaviours can be interpreted in two ways, either with a population of unresolved blazars, that on the other hand should have different characteristics than these resolved in the *Fermi*-LAT catalog, or with an additional contributor to the UGRB, as, e.g., a dark Weakly Interactive Massive Particle (WIMP). The CC analysis of *Fermi* data with the forthcoming Year 3 and Year 5 DES data sets, and improvements in modelling the blazar population will likely clarify the nature of the signal that we have detected detected.

For a better characterization of the unresolved γ-ray emission of the Local Universe, where a DM signal is expected to have the largest signal-to-background ratio, we measure the angular CC of the 2MPZ catalog with *Fermi*-LAT skymaps. The 2MPZ catalog contains about one million of galaxies with a median redshift $z = 0.07$. The cosmological volume probed by 2MPZ powers only about 10% of the total unresolved γ-ray background. Despite this small fraction, the CC technique enables us to study the composition of such emission. The null hypothesis, i.e., the absence of correlation between the two datasets, is excluded at a statistical confidence larger than 99.99%. To understand the origin of this correlation, we split the 2MPZ catalog into subsamples using redshift, K-band luminosity (taken as a tracer of the object mass) and B-band luminosity (taken as a tracer of the star formation rate of the object) as markers. We find misaligned AGN [mAGN] to be the most likely contributor of the bulk of the signal. The normalization of this contribution is such that the extrapolation to higher redshift makes

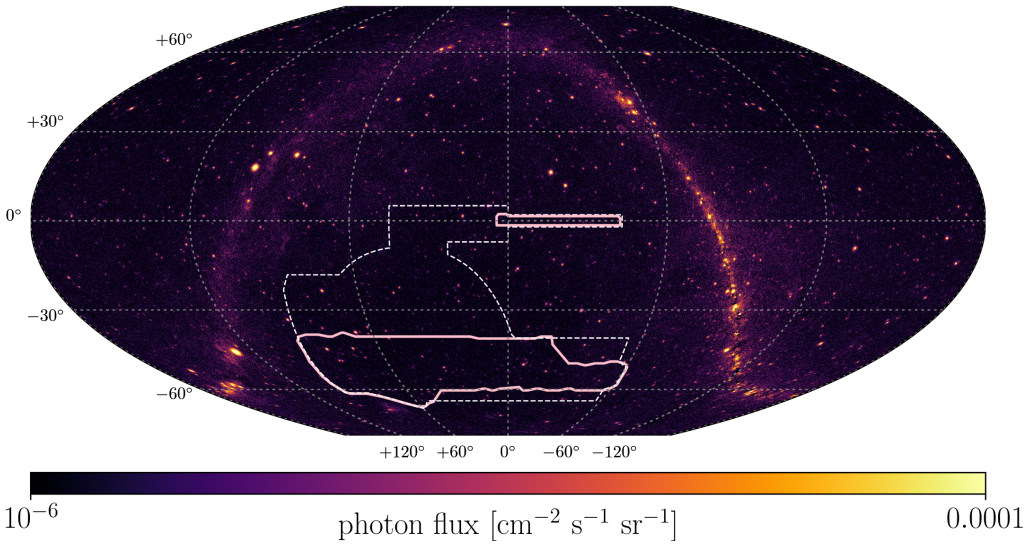

Fig. 1. DES Y1 (solid) and final (dashed) sky coverage superimposed on the *Fermi*-LAT γ-ray map for photons in the 1-10 GeV energy range, adapted from (Ammazzalorso et al. 2020).

mAGN emission compatible with explaining the majority of the UGRB at GeV energies. Star forming galaxies appear to be a subdominant component in our measurement at low redshift. Nevertheless, the derived bounds allow them to still be a significant component of the UGRB at higher redshift. The energy spectrum of the 2MPZ $\times$*Fermi* CC somewhat favors the presence of a blazar-like component at high-energies. On the other hand, the contribution is rather featureless and an improvement in understanding the link between IR and γ-ray luminosity for faint blazars is mandatory to fully assess this point. Finally, we evaluate the possible contribution of a particle DM signal in this CC. The 95% confidence level bounds on the DM annihilation rates reach close to the "thermal" rate for DM mass of 10 GeV for $b\bar{b}$, $\tau^+\tau^-$ and W^+W^- annihilation channels (while an order of magnitude weaker bound is found for $\mu^+\mu^-$) and then increasing with a nearly linear trend for higher masses. Interestingly, when considering samples where the DM evidence is expected to increase (namely, correlation with objects at low-z, with high-mass, and low level of star formation), we see a slightly more pronounced peak in the likelihood for the DM contribution. Currently, the statistical significance of this effect is however low.

Alternatively to the CC analysis, one can consider the auto-correlation of the γ-ray sky. We perform a measurement of the UGRB auto-correlation angular power spectrum based on eight years of *Fermi*-LAT Pass 8 data products. The analysis is designed to be robust against contamination from resolved sources and noise systematics. The sensitivity to sub-threshold sources is greatly enhanced with respect to previous measurements. We find evidence (with $\sim 3.7\sigma$ significance) that the scenario in which two classes of sources contribute to the UGRB signal is favored over a single class. A double power law with exponential cutoff can explain the anisotropy energy spectrum well, with photon indices of the two populations being 2.55 ± 0.23 and 1.86 ± 0.15, see Fig. 2.

3. X-rays and sterile neutrinos

The cosmological X-ray emission associated to the possible radiative decay of sterile neutrinos is composed by a collection of lines at different energies. For a given mass, each line corresponds to a given redshift. Exploiting this property, we investigate the cross-correlation

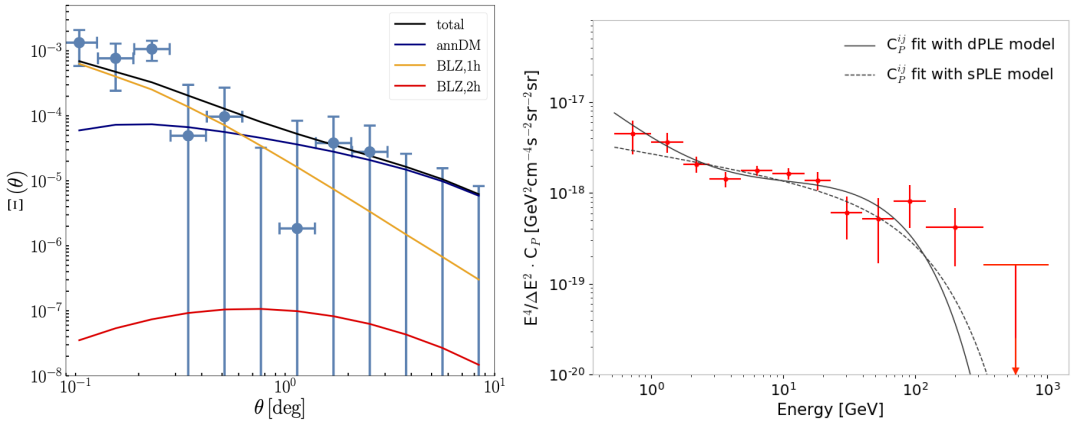

Fig. 2. Left: Angular cross-correlation of DES Y1 cosmic shear with the UGRB observed by the *Fermi*-LAT telescope, adapted from (Ammazzalorso et al. 2020). Right: UGRB auto-correlation, adapted from (Ackermann et al. 2018).

of the X-ray emission with catalogs of galaxies tracing the dark matter distribution at different redshifts.

We perform the line intensity mapping analysis for the eROSITA (Predehl et al. 2021) and Athena (Nandra et al. 2013) X-ray telescopes, and considering current and near future photometric and spectroscopic galaxy surveys. Our main results are summarized in Fig. 3 (left).

With gray lines, we report also the lower limit given by the requirement that sterile neutrino accounts for all the DM in the Universe in the case of resonant production and for a lepton asymmetry of $L = 7 \times 10^{-5}$ (solid) and $L = 2.5 \times 10^{-3}$ (dashed, the maximum value allowed by BBN).

The eROSITA satellite, which is currently in operation, will be able to slightly improve existing bounds and test the DM interpretation of the 3.55 keV line excess. Thanks to the improved effective area, the Wide Field Imager (WFI) on board of the future Athena satellite will test a much larger and unexplored region of the parameter space. The line intensity mapping technique can be fully exploited combining the superior spectral resolution of the second Athena instrument, the X-ray Integral Field Unit (X-IFU), with spectroscopic surveys, like DESI (DESI Collaboration et al. 2016). On the other hand, the limited field of view of the X-IFU leads to sensitivities slightly worse than in the case of analyses with the WFI. Despite this, if a positive signal will be detected, the X-IFU spectroscopic observations can allow a more robust identification and characterization of the DM cosmological line.

Summarizing, we find that, in the near future, X-ray line intensity mapping can become a suitable technique to search for a sterile neutrino decay signal, complementary to observations of individual targets.

4. The near-infrared and ALPs

The extragalactic background light is comprised of the cumulative radiation from all galaxies across the history of the universe. The angular power spectrum of the anisotropies of such a background at near-infrared frequencies lacks of a complete understanding and shows a robust excess which cannot be easily explained with known sources. Dark matter in the form of axion-like particles (ALPs) with a mass around the electronvolt will decay into two photons with wavelengths in the near-IR band, possibly contributing to the background intensity. We compute the near-IR background angular power spectrum including emissions

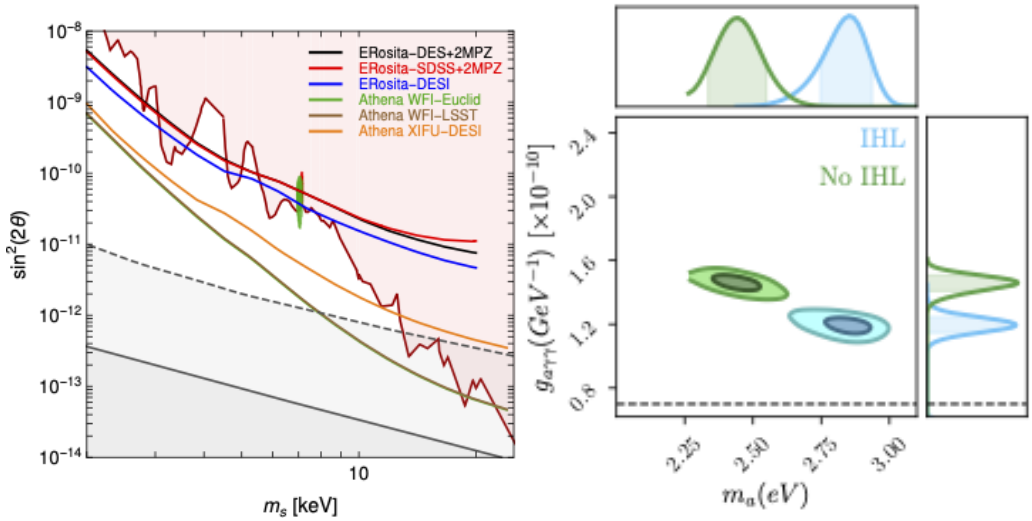

Fig. 3. Left: Projected sensitivity from the line intensity mapping of the sterile neutrino signal, adapted from (Caputo et al. 2020). Right: Preferred region in the ALP parameter space, in order to explain the the near-infrared background excess through ALP-photon decay, adapted from (Caputo et al. 2021).

from galaxies, as well as the contributions from the intra-halo light ad ALP decay, and compare it to observations in the optical and infrared bands. We find that the preferred values for the ALP mass and ALP-photon coupling to explain the excess, shown in Fig. 3 (right) are in tension with star cooling data and observations of dwarf spheroidal galaxies.

5. Primordial black holes

PBHs may constitute a significant part of DM. We derived new limits on the PBH abundance, from a comprehensive analysis of high-resolution high-redshift Lyman-α forest data (Murgia et al. 2019). Poisson fluctuations in the PBH number density induce a small-scale power enhancement with respect to the standard CDM prediction. Using hydrodynamic simulations, we obtained an upper limit on the PBH mass of $f_{PBH}\, M_{PBH} = 60\, M_\odot$ at 95% C.L. (with $f_{PBH} = \Omega_{PBH}/\Omega_{DM}$), when a Gaussian prior on the reionization redshift is imposed, preventing its posterior distribution from peaking on very high values, which are disfavored by the most recent estimates obtained both through CMB and intergalactic medium observations. Such a bound weakens to $f_{PBH}\, M_{PBH} = 170\, M_\odot$ when a conservative flat prior is instead assumed. Both limits significantly improve on previous constraints based on Lyman-α data. Bounds to non-monochromatic PBH mass distributions are also derived, ruling out large portions of the parameter space for some of the most viable PBH extended mass functions.

6. Exploring the physics of the missing baryons

Searches of the MB in the WHIM have, so far, largely relied upon the detection of specific absorption lines in the spectra of background, bright X-ray sources. Integral field spectroscopy performed with instruments like Athena X-IFU will provide us with the possibility to perform intensity mapping analysis using the same lines in emission. We use state-of-the art hydrodynamical simulations to test this technique and assess its effectiveness

in probing the WHIM properties and in revising the baryon budget in the local Universe. Our dataset is the suite of 4233 "CAMELS" (Villaescusa-Navarro et al. 2020) simulations designed to provide predictions for a large range of cosmological and stellar feedback models. Our analysis focuses on two relevant cosmological parameters, the mean matter density, $\Omega_{\rm m}$, and the clustering amplitude, σ_8. The stellar feedback models are characterized by four parameters that regulate the energy release from Supernovae and AGNs. We exploit this large dataset to assess the robustness of the WHIM predictions to model uncertainties, especially for the stellar feedback part. The parameter space probed by the CAMELS dataset is, in fact, too wide for our goals. Therefore, we restrict our analysis to a subset of models that are not ruled out by observations. We consider the following three sub-sets:

- **IllustrisTNG-CV**. This set consists of 27 independent realizations of the same fiducial ΛCDM cosmology with $\Omega_{\rm m}^{\rm fid} = 0.3$ and $\sigma_8^{\rm fid} = 0.8$. Stellar feedback parameters are also the same in all realizations. These simulations were performed with the AREPO hydrodynamical code in a computational box of size $25\,h^{-1}$ Mpc.
- **SIMBA-CV**. Is a twin set of 27 realizations of the same model, with the same initial conditions, in the same boxes but performed with a different numerical code: GIZMO.
- **IllustrisTNG-LH**. This set consists of 63 realizations of different models. The cosmological parameters are chosen to be similar to that of the fiducial model (with relative differences in their values smaller than 0.05). Stellar feedback parameters span, instead, a large range of values.

Since the intergalactic medium is expected to become warm and hot only at recent epochs we limit the analysis to three simulation snapshots at $z = 0.54, 0.27$ and 0.03. Moreover we focus on the two most prominent WHIM emission lines, the OVII triplet at 0.57 keV and the OVIII singlet at 0.653 keV. We use the simulated gas particles in each of these snapshots to simulate the surface brightness maps of both lines and, to obtain realistic predictions, we set the energy and angular resolution equal to those of the X-IFU, i.e., $\Delta E = 2.5$ eV and $\theta_{\rm res} = 5$ arcsec (Nandra et al. 2013). The thickness of each map is set by the energy resolution of the instrument. At the redshift of the three snapshots, the thickness is 14.4, 13.8 and 12.7 h^{-1} Mpc. Similarly, the the X-IFU angular resolution sets the number of pixels in each map, which is equal to 732, 1360 and 13838, respectively.

To generate the surface brightness maps, we feed the density, temperature and chemical composition of the gas particles into the `pyXsim` code (ZuHone et al. 2016) to obtain the X-ray spectrum emitted by each gas particle under the assumption of collisional ionization equilibrium. We then interpolate the resulting line emissivity at the points of a cubic grid with a mesh size that matches the X-IFU angular resolution at the redshift of the snapshot. From this we compute the line surface brightness in each pixel of a two-dimensional map (Bertone et al. 2010).

Fig. 4 shows the OVII surface brightness maps obtained from three snapshots of one **IllustrisTNG-CV** realization among the 27 available. Having defined the WHIM as the gas with overdensity $\delta < 1000$ and temperature $10^5\ {\rm K} < T < 10^7\ {\rm K}$, the maps include contribution from the WHIM gas particles only. The brightness levels are color-coded according to the reference bar shown in the plot. Green circles are drawn at the angular position of the massive halos in the simulation. Their size is proportional to the halo mass. As expected line emission is concentrated around halos and along the connecting filaments. In the bottom panel we show the same maps after excluding pixels in which the line surface brightness is fainter than 0.1 photons ${\rm cm^{-2}s^{-1}sr^{-1}}$, i.e. the threshold above which X-IFU is expected to detect emission lines with a significance larger than 3-σ after a 100 Ksec observation.

These maps suggest that next generation satellite missions like Athena will indeed be able to detect the MB in the elusive WHIM associated to massive DM halos populated by galaxies. The WHIM-halos proximity suggests that a cross-correlation analysis between

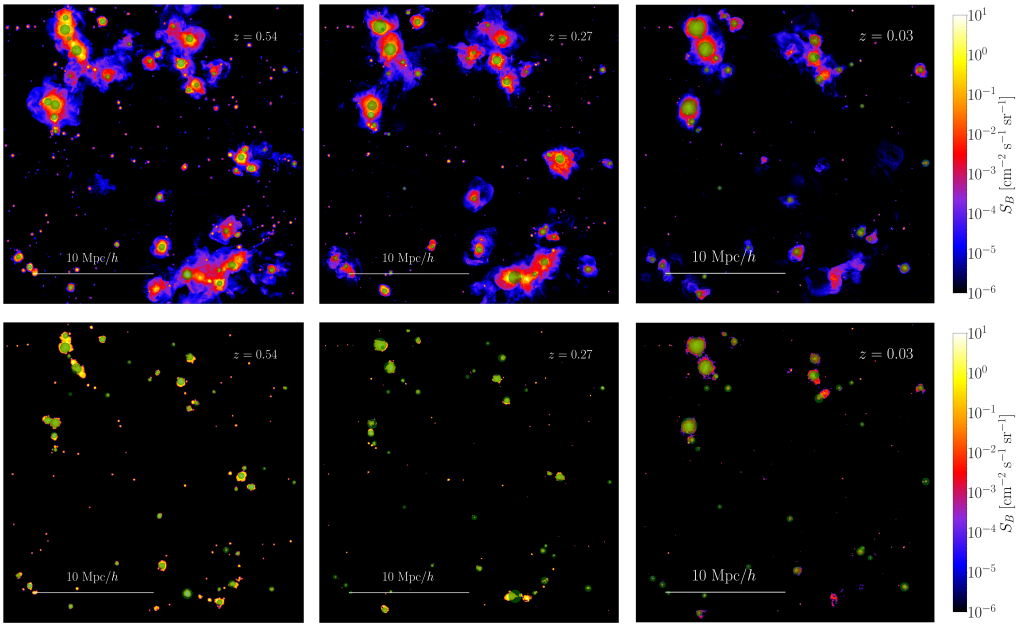

Fig. 4. Top panels: OVII surface brightness maps from one simulation of the **IllustrisTNG-CV** set, estimated at three different redshifts, $z = 0.54, 0.27, 0.03$ (left to right). Green circles mark halos of $M \geq 10^{12}\ M_{\odot}/h$. The size of the circle is proportional to their virial radius. Bottom panels: same maps excluding pixels with surface brightness fainter than 0.1 cm^{-2}s^{-1}sr^{-1}

galaxy redshift catalogs and X-ray surface brightness maps at selected wavelength may be a good strategy to detect the MB, trace their spatial distribution and constrain their physical properties. The plot also depicts the evolution of the WHIM traced by the OVII line. The gas, initially distributed around small halos and along the connecting filaments becomes more and more concentrated around increasingly larger halos that form through the merging process.

To characterize more quantitatively the WHIM-halo spatial distribution and their mutual dynamics we estimate the spatial 2-point CC function of oxygen emitters and halos in the simulation. The upper panel of Fig. 5 shows the monopole moment of the OVII-halo CC function at $z = 0.27$ for different simulation sets. We only consider emission from WHIM particles. The thick curve shows the average CC computed from the 27 **IllustrisTNG-CV** realizations together with its 1-σ scatter (shaded area). At small separation the CC exhibits a typical power law behavior. However, the CC becomes negative at relatively small scales ($\sim$ 10 Mpc h^{-1}). This transition is a manifestation of the so-called integral constraint that follows directly from mass conservation and forces the integral of the 2PCF to vanish over the simulated volume. The behavior of the quadrupole moment (bottom plot) is genuine and, therefore, more interesting. The fact that it is non zero reflects the apparent clustering anisotropy induced by peculiar motions, commonly known as redshift distortion. Its sign reveals the relative dynamical state of the WHIM and the halos. The positive quadrupole at small separation reflects the incoherent motions of the gas particles near halos. Moving away from the halo centers the quadrupole become negative revealing that velocities become more coherent, tracing the infall motion of the gas towards massive structures.

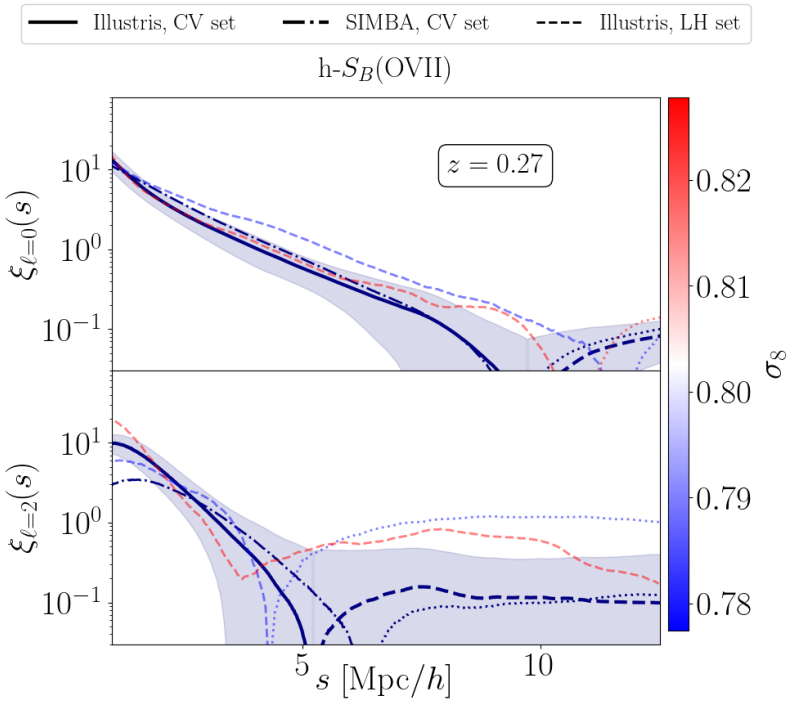

Fig. 5. Three-dimensional halo-OVII cross correlation function monopole (top panel) and quadrupole (bottom panel) at $z = 0.27$. Thick solid and dot-dashed curves show the average CC of the **IllustrisTNG-CV** and **SIMBA-CV** realizations. Dashed and dotted styles are used for negative values. The shaded area shows the 1-σ scatter among the realizations. The colored curves show the two most extreme CCs measured in the **IllustrisTNG-LH** set. They are color coded according to their σ_8 values indicated in the color bar.

The other curves in the plot show the predictions of the other simulation sets: the **SIMBA-CV**, for which we show the mean CC (dot-dashed), and the **IllustrisTNG-LH** set, from which we have selected two simulations performed with extreme stellar feedback models but with similar cosmological parameters (red and blue dashed lines).

While the CC of the **SIMBA-CV** model is similar to the reference **IllustrisTNG-CV** case, the two dashed curve are significantly different. In particular the quadrupole of the red dashed curve is always positive. This means that the gas dynamics is dominated by incoherent motions, randomized by the intense feedback and energy injection. It is clear from these results that this type of CC analysis will provide precious information on the physics of the WHIM.

The CC function shown in Fig. 5 is computed from the three dimensional distribution of the OVII emissivity estimated at the nodes of finely spaced cubic grid. The energy resolution of the detector provides a natural smoothing scale along the line of sight that, in the case of X-IFU, is too large to allow one to trace the spatial distribution of the gas. One can, nevertheless, perform a tomographic analysis by computing the angular CC functions of the surface brightness maps in redshift slices of appropriate thickness.

The results of this approach are shown in Fig. 6. In this plot we show the projected (rather than the angular) CC function of both OVII-halos and OVIII-halos (left and central

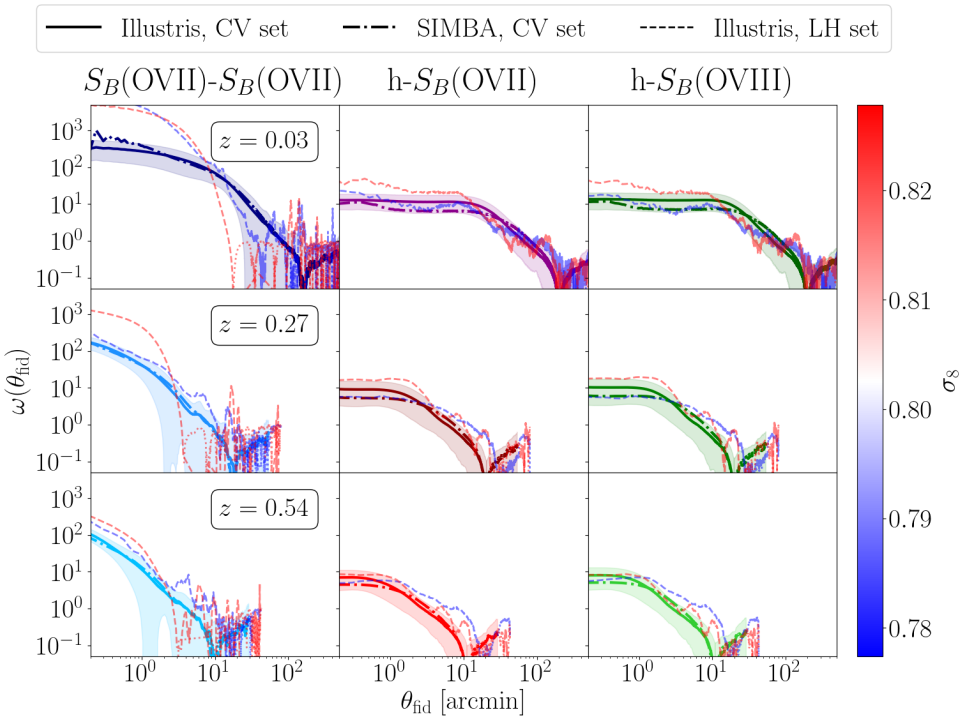

Fig. 6. Angular CCs for OVII-OVIII (left panels), halos-OVII (central), halos-OVIII (right) at increasing redshifts (from top to bottom) indicated in the plots. Model predictions are the same as in Fig. 5 and plotted with the same linestyles.

panels) together with the OVII-OVIII cross correlation function. These quantities are computed at three different redshifts, as indicated in the panels at the top, central and bottom rows. For consistency we use the same linestyles as in Figure 5. The size of the angular bin (5 arcsec) is set by the X-IFU resolution. Unsurprisingly, the CC functions of the various models show the same qualitative differences seen in the CC monopole in Fig. 5. There are, however, some new and quite surprising results: the similarity between the OVII-halo and OVIII-halo CC functions, the fact that the clustering length, defined as the scale at which the CC becomes negative, increases with time and, finally, the fact that both CC functions have a core-like shape at small separations. The core-like feature is not merely induced by projection effects, as otherwise a similar shape would be observed in the OVII-OVIII CC. It is determined, at least in part, by the depletion of OVII and OVIII in the central regions of the halos in which temperature and density are too large for these ions to form.

Another useful summary statistics is the probability distribution function of the oxygen emitters as a function of the line surface brightness. This quantity is commonly dubbed LogN-LogS and can be estimated from the surface brightness maps by simply counting pixels above a given brightness threshold. We plot the cumulative LogN-LogS distribution in Fig. 7 for OVII (left), OVIII (center) and for OVII+OVIII at different redshifts (bottom to top). In the OVII+OVIII case we count the pixels in which both OVII and OVIII surface brighthenss is above threshold. We consider the same models as in the previous plots

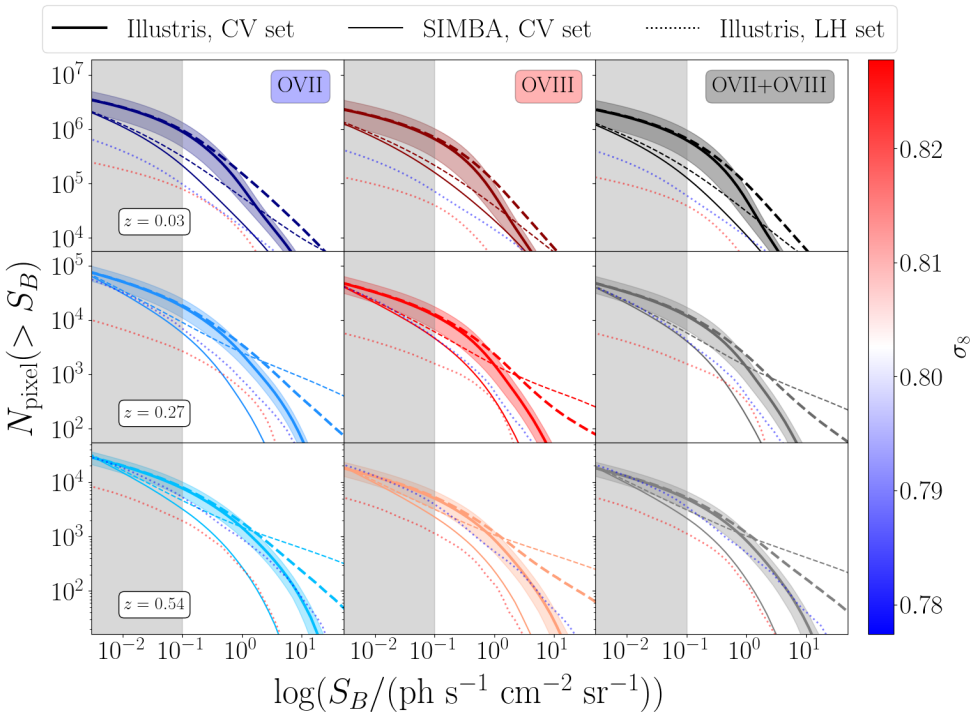

Fig. 7. LogN-LogS for OVII (left), OVIII (center) and OVII+OVIII (right) emitters at three different redshift values, 0.03 (top), 0.27 (center) and 0.54 (bottom). Thick solid curve and shaded areas show the average and the 1-σ scatter among the **IllustrisTNG-CV** realizations. Only WHIM particles are considered. Thick dashed lines account for lines counts from all gas particles. Thinner curves show the **SIMBA-CV** case. Dotted curves show the two most extreme models of the **IllustrisTNG-LH** set. The gray area is shown for reference and includes surface brightness values below Athena X-IFU detection threshold for a 100 Ks observation.

but use different linestyles. Thick continuous curves indicate the average LogN-LogS for the **IllustrisTNG-CV** model contributed by WHIM only. Thick dashed curve account for contributions from all the gas particles, including the WHIM. For the **SIMBA-CV** case we use thin curves but same styles. Finally, the blue and red dotted curves show the same two extreme cases drawn from the **IllustrisTNG-LH** dataset. The sheer number of emitters in these two extreme cases is significantly smaller than in both the reference and **SIMBA-CV** models. This difference illustrates the impact of an efficient heating and stellar feedback mechanism that pushes away and fully ionize the oxygen atoms.

7. Conclusions

In this report, we have described the results of two projects that share both a common scientific goal, the quest for dark components in the cosmos, and a common strategy, their indirect detection by means of cross correlation with the visible matter.

The dark components we have focused on have, however, very different properties. The very existence of the first one, the DM, is still hypothetical. In this work we join the effort of detecting its presence and unveiling its nature and we do so by searching the high energy Universe. We looked for DM signatures in the γ-ray sky maps produced by the *Fermi*-

LAT telescope. To enhance the low signal-to-noise of the DM and to minimize the spurious contribution of astrophysical sources and foregrounds, we have cross correlated UGRB maps with known tracers of the gravity potential such as weak lensing and galaxy redshift catalogs. The CC analysis proved to be a precious tool for unveiling the nature of the unresolved astrophysical γ-ray sources and, in so doing, providing constraints on the mass and cross section of WIMP DM candidates.

We also explored the possibility to search for characteristic line emission from sterile neutrinos decay in the X-ray band. We found that ongoing satellite missions like eROSITA will improve existing constraints. And that further improvements are expected from the complementary X-ray intensity mapping approach that will be carried out with next generation Integral Field Units like X-IFU.

The second dark component is not exotic. MB are standard model particles that have so far largely evaded detection because of their low density and high temperature. Despite the recent claims of MB detection, a detailed account of the baryon budget and a complete characterization of the MB is still to be achieved. In this work we have used state-of-the-art hydrodynamical simulations to assess the possibility to study the property of the WHIM, where a large fraction of the MB are expected to reside, via emission line intensity mapping in the soft X-ray band. In analogy with the sterile neutrino case, the idea is to perform CC analyses with WHIM tracers to isolate and get rid of spurious signals generated by non-WHIM sources. We found that combining CC analyses with other summary statistics (auto correlation, emitter counts) constitutes a promising strategy to tackle the MB problem with next generation X-ray satellite missions.

Affiliations

[6] INFN, Sezione di Torino, via P. Giuria 1, I–10125 Torino, Italy

[7]INFN – Istituto Nazionale di Fisica Nucleare, Sezione di Trieste, Via Valerio 2, I–34127 Trieste, Italy

[8] INAF, Osservatorio Astrofisico di Torino, strada Osservatorio 20, I-10025 Pino Torinese, Italy

[9] Institute of High Energy Physics, Chinese Academy of Sciences, Beijing 100049, China

[10] School of Physical Sciences, University of Chinese Academy of Sciences, Beijing 100049, China

[11] Department of Astronomy, Beijing Normal University, Beijing 100875, China

[12] Dipartimento di Fisica, Universitá di Genova

Acknowledgements. We all acknowledge support from Research grant "Deciphering the high-energy sky via cross correlation" and "Unveiling Dark Matter and missing baryons in the high-energy sky" funded by the agreement ASI-INAF n. 2017-14-H.0. EB and MR are further supported by Research grant "From Darklight to Dark Matter: understanding the galaxy/matter connection to measure the Universe" No. 20179P3PKJ funded by MIUR. MR acknowledges support by: 'Departments of Excellence 2018-2022' grant awarded by the Italian Ministry of Education, University and Research (MIUR) L. 232/2016; Research grant TAsP (Theoretical Astroparticle Physics) funded by INFN EB is also supported by ASI-INAF agreement n. 2018-23-HH.0 "Scientific Activity for the Euclid Mission Phase D" and INFN Project "InDark".

References

Abbott T. M. C., Abdalla F. B., Alarcon A., Aleksić J., Allam S., Allen S., Amara A., et al., 2018, PhRvD, 98, 043526. doi:10.1103/PhysRevD.98.043526

Ackermann, M., et al. Unresolved Gamma-Ray Sky through its Angular Power Spectrum. *Phys. Rev. Lett.* **121**, 241101 (2018)

T. Abbott *et al.* [DES], Mon. Not. Roy. Astron. Soc. **460** (2016) no.2, 1270-1299.

J. Zuntz *et al.* [DES], Mon. Not. Roy. Astron. Soc. **481** (2018) no.1, 1149-1182

B. Hoyle *et al.* [DES], Mon. Not. Roy. Astron. Soc. **478** (2018) no.1, 592-610

S. Ammazzalorso, N. Fornengo, S. Horiuchi and M. Regis, Phys. Rev. D **98**, no. 10, 103007 (2018)

S. Ammazzalorso *et al.* [DES], Phys. Rev. Lett. **124** (2020) no.10, 101102

Bertone S., Schaye J., Dalla Vecchia C., Booth C. M., Theuns T., Wiersma R. P. C., 2010, MNRAS, 407, 544. doi:10.1111/j.1365-2966.2010.16932.x

Camera, S., Fornasa, M., Fornengo, N., & Regis, M. A Novel Approach in the Weakly Interacting Massive Particle Quest: Cross-correlation of Gamma-Ray Anisotropies and Cosmic Shear. *Astrophys. J.* **771** L5 (2013)

A. Caputo, M. Regis and M. Taoso, JCAP **03** (2020), 001

A. Caputo, A. Vittino, N. Fornengo, M. Regis and M. Taoso, JCAP **05** (2021), 046

R. Cen and J. P. Ostriker, Astrophys. J. **514** (1999), 1-6

Cuoco, A., Xia, J.-Q., Regis, M., et al. Dark matter searches in the gamma-ray extragalactic background via cross-correlations with galaxy catalogues. *Astrophys. J. Suppl.* **221**, 29 (2015)

DESI Collaboration, Aghamousa A., Aguilar J., Ahlen S., Alam S., Allen L. E., Allende Prieto C., et al., 2016, arXiv, arXiv:1611.00036

M. Fukugita, C. J. Hogan and P. J. E. Peebles, Astrophys. J. **503** (1998), 518

O. E. Kovács, Á. Bogdán, R. K. Smith, R. P. Kraft and W. R. Forman, Astrophys. J. **872** (2019) no.1, 83

K. Nandra, D. Barret, X. Barcons, A. Fabian, J. W. d. Herder, L. Piro, M. Watson, C. Adami, J. Aird and J. M. Afonso, *et al.* [arXiv:1306.2307 [astro-ph.HE]].

F. Nicastro, J. Kaastra, Y. Krongold, S. Borgani, E. Branchini, R. Cen, M. Dadina, C. W. Danforth, M. Elvis and F. Fiore, *et al.* Nature **558** (2018), 406

Predehl P., Andritschke R., Arefiev V., Babyshkin V., Batanov O., Becker W., Böhringer H., et al., 2021, A&A, 647, A1. doi:10.1051/0004-6361/202039313

Murgia, R., Scelfo, G., Viel, M., et al. Phys. Rev. Lett. **123** (2019), 071102. doi:10.1103/PhysRevLett.123.071102

M. Regis, J. Q. Xia, A. Cuoco, E. Branchini, N. Fornengo and M. Viel, Phys. Rev. Lett. **114** (2015) no.24, 241301

J.M. Shull, B.D. Smith, C.W. Danforth, Astrophys. J. **759** (2012), 1-23

Takei Y., Ursino E., Branchini E., Ohashi T., Kawahara H., Mitsuda K., Piro L., et al., 2011, ApJ, 734, 91. doi:10.1088/0004-637X/734/2/91

F. Villaescusa-Navarro, D. Anglés-Alcázar, S. Genel, D. N. Spergel, R. S. Somerville, R. Dave, A. Pillepich, L. Hernquist, D. Nelson and P. Torrey, *et al.* Astrophys. J. **915** (2021), 71

J.A. ZuHone, E.J. Hallman, ADS-NASA

XRISM Science Team, 2020, arXiv, arXiv:2003.04962